UNIVERSITY OF OKLAHOMA GRADUATE COLLEGE

THE EFFECTS OF LEGACY SEDIMENT ON MICROBIALLY-MEDIATED REDOX CYCLING IN AN ISOLATED FLOODPLAIN

A THESIS

SUBMITTED TO THE GRADUATE FACULTY

in partial fulfillment of the requirements for the

Degree of

MASTER OF SCIENCE

By Dodger Stankewitz

Norman, Oklahoma

2025

THE EFFECTS OF LEGACY SEDIMENT ON MICROBIALLY-MEDIATED REDOX CYCLING IN AN ISOLATED FLOODPLAIN

A THESIS APPROVED FOR THE

SCHOOL OF GEOSCIENCES

BY THE COMMITTEE CONSISITING OF

Dr. Caitlin A. Hodges, Chair

Dr. Andrew S. Elwood Madden

Dr. Michael J. Soreghan

Table of Contents

Abstract

Post-settler colluvium or legacy sediment is a layer of fine sediment that has accumulated through improper farming practices of colonial settlers. The legacy sediment is eroded from hillslopes and deposited down onto active soil and covers it up. We hypothesized that an additional layer of material would modify the concentration of oxygen in the soil and as a result, affect the redox cycles of major nutrients. We constructed soil mesocosms and subjected them to varying degrees of oxygen concentrations and gravimetric water content via an anaerobic chamber to simulate the unique conditions of our field site. The iron and manganese in the mesocosms exhibited behavior of direct electron transfer, with the more electropositive manganese acting as an electron acceptor for iron oxidation. The more soluble reduced manganese was able to facilitate redox reactions while stable in the anoxic treatments. Additionally, the increased reduction of iron over time is driven by reductive-dissolution of iron oxides that recrystallize into structurally weak amorphous iron oxides that are more readily reduced. The anaerobic chamber provided a pathway for nitrogen fixation into nitrate which was reduced by microbial organisms with iron and manganese acting as electron donors. There was overall significant fractionation between the nutrient concentrations of the oxygen states, especially with manganese and nitrate. The carbon contents of the mesocosms that had any anoxia were all increased over the oxic, with a noticeable increase in nitrogen as well. Overall, the results indicate that manganese is exerting a larger control on the redox reactions in the buried soils than previously thought, and the method of destructive sampling of a lab-controlled buried soil is viable and scalable.

Introduction

Soil Carbon

Soils are a massive organic carbon (C) sink, and store over 75% of Earth's terrestrial carbon (Johnston et al., 2004). Soils store nearly 5x the amount of carbon stored in vegetation, making them an essential regulator for the Earth's carbon budget (Lal, 2004). However like most of the earth system, the pools of actively cycling carbon, the atmosphere, soils, vegetation, and the oceans are heavily intertwined. Atmospheric carbon dioxide (CO_2) is first taken up by vegetation and nearly half is released back as CO2 through respiration with resulting in a net primary production of around 60 Pg C/year (Janzen, 2004). The plants decay over time through decomposition and carbon enters the soil as biomass. Decomposition is simply the breakdown of complex organic substances into much simpler components that can be both organic and inorganic. Soil microorganisms are critical to the global carbon cycle because they control the fate of the organic carbon in plant biomass (Johnston et al., 2004). First, the microorganisms facilitate the decomposition of plant biomass, using the organic matter as an energy source for respiration. This heterotrophic respiration is often the largest flux of carbon from soils, nearly equaling the rate of carbon fixation by primary producers (Janzen, 2004). Some of the plant biomass is also assimilated by microorganisms, and the resulting microbial biomass contributes to the stable pool of soil carbon.

Soil Organic Matter (SOM) is a broad term that refers to the organic components of soil. SOM is made up of living components including soil microorganisms, plant roots, and fauna. It also contains nonliving organics such as leaf litter, actively decomposing

organic matter, and humus (Cotrufo and Lavallee, 2022).Soil Organic Matter is found in three “states” in soils: Particulate Organic Matter (POM), Dissolved Organic Matter (DOM), and Mineral-Associated Organic Matter (MAOM). POM is comprised of structural carbon compounds and is protected in soils through aggregates. POM is much more prone to disturbances than MAOM and has a much lower residence time in soils (1 - 50 years) (Cotrufo and Lavallee, 2022). DOM is organic matter that is in solution in soils. It is product of microbial respiration and contributes to the formation of MAOM. MAOM are microbial products that are chemically bonded to mineral surfaces. MAOM is less complex in structure than POM and has a much longer residence time in soils (10-1000 years) due to its natural protection in the mineral.

Iron and Manganese Cycling in Soils

Iron is a micronutrient in soils and living organisms that is essential for growth and development. In multicellular animals, iron forms an organic complex called heme that forms into hemoglobin, a vital protein responsible for carrying oxygen through the blood (Konhauser et al., 2011). In plants and soils, iron facilitates three fundamental reactions for life, photosynthesis, cellular respiration, and synthesis of chlorophyll. Iron is an essential micronutrient for almost all living organisms because it plays a critical role in metabolic processes such as DNA synthesis, respiration, and photosynthesis. (Rout and Sahoo, 2015). Additionally, Iron is important because it can fluctuate between two redox states: insoluble, crystalline Fe (III) in the form of (hydr)oxides and bioavailable Fe (II). As such, some microorganisms can use Fe (III) as a terminal electron acceptor for respiration. However, this reaction yields less energy than aerobic respiration and is only thermodynamically favorable in the absence of oxygen, nitrate,

and manganese. In a fluctuating redox environment such as a soil or even a larger ecosystem like a wetland, this “iron redox wheel” is strongly coupled with the cycling of multiple other essential macronutrients, oxygen, nitrogen, sulfur, and most importantly, carbon (Li et al., 2012a). The reduction of iron is facilitated with electron donation, or oxidation from another species in the environment, commonly hydrogen gas, organic carbon, methane, or additional simple or complex organic molecules (Konhauser et al., 2011).

Manganese is one the most abundant transition metals in Earth’s crust and is actively used by microbial organisms to cycle important macronutrients in soils (Anderson et al., 2011). Manganese exists primarily in three redox states in soils: crystalline-insoluble Mn (III) and Mn (IV), and soluble Mn (II). In low-O2 conditions commonly created through flooding, manganese is commonly used as a terminal electron acceptor for microbial respiration. The process of manganese reduction through anoxia is well understood in paddy soils (Haque et al., 2015). While they are typically seen filling similar roles in a system, there are two key differences between iron and manganese. Firstly, manganese is more electropositive than iron and as a result, has a higher redox potential. Secondly, reduced manganese is generally more soluble than iron and is less easily oxidized than reduced iron (Krauskopf, 1957). Upon flooding, conditions in the soil become reducing and the soils are able to store a significant portion of SOC that is quite susceptible to microbial decomposition upon reoxygenation (Li et al., 2021). As flooded soils drain and begin to reoxygenate, the subsequent oxidation of iron and manganese can produce reactive oxygen species that are critical in breaking down larger, more complex organic compounds in soils (Jones et al., 2018).

Organic matter accumulates in low-O2 environments as the reduction of Mn (IV) and Fe (III) is coupled with the oxidation of organic matter, resulting in less efficient oxidation of carbon (Li et al., 2012b). When these metal oxides are reduced in soils, the ions and colloids trapped in the minerals are released into solution and are available for uptake by roots (Stucki, 2011). Due to their ability to fluidly transition between redox states, iron and manganese cycling is heavily affected by outside factors that can modify or change a soil's ability to freely interact with the biota and atmosphere

Legacy Sediment

The Earth underwent extreme geomorphological change through its history, from incredibly hot with widespread volcanism in the Hadean to nearly frozen solid in the Neoproterozoic. Since humanity began to modify the land, we have been producing anthropogenic alluvium or legacy sediment. Legacy sediment behaves like any other non-anthropogenic sediment and as such, the same large-scale concepts that are used to explain the way sediments travel into catchements can be used to explain the life cycle of legacy sediment (James, 2018). Bottom-land alluvium produced through colluvial cascades preserves an extensive record of anthropogenic land use that can be traced back to nearly 10,000 B.C. in the Neolithic (Allan, 2021). Large scale sedimentation events were preceded by agricultural revolutions associated with many of the great historic civilizations including the Greeks, Romans, Assyrians, Mayans, etc. (Allan, 2021). The effects felt from agriculture, mining, and the construction of large structures ultimately compound in rivers and floodplains, since they are the medium by which the majority of sediment is transported across earth.

As society has developed, the demand for resources such as food, water, wood, rock, and metals has increased with the growing population. Humans are spread out across the world and shaping the natural environment to support more and more life. Check dams to change the shape of rivers have impounded large amounts of sediment and drastically reduced the recharge of shorelines (Wohl and Merritts, 2007). Logging operations have deforested large parcels of land and have had cascading effects on the wildlife through land use change (James, 2018). Legacy sediment not only has a significant impact on the sedimentary rock cycle, but it also impacts the nutrient cycling of terrestrial ecosystems. Increased sedimentation can not only transport additional nutrients from source to sink, but can impede a system's ability to cycle essential nutrients (carbon, nitrogen, phosphorous, oxygen, and iron) by increasing the amount of clay present in the system (Swinnen et al., 2020). The field site that this research was conducted at is an abandoned farm that has been heavily tilled and terraced, producing a pronounced layer of legacy sediment that now overlies the organic rich soil of the area (Figure 1). Research into the role that humans play in the geomorphology of our environment and modern critical zones can give us a more accurate understanding of some of the unintended effects of modern civilization.

Figure 1: cross-section of the stream bank at the KAEFS floodplain. The organic-rich A horizon characteristic of the mollisols in the region is buried beneath a layer of clay sediment. The sediment is derived from erosion that was accelerated by significant cultivation and pasturing. The burial is most pronounced at the bank and reaches a maximum burial depth of 50cm.

Research Motivation and Hypothesis

With this project, we examine the relationship between anthropogenic legacy sediment and the complex biogeochemistry that actively cycles nutrients through the subsurface. We look at redox transition zones in legacy sediment that actively cycle iron (Fe) and manganese (Mn) that are known to facilitate the flow of carbon. Redox transition zones are heavily dependent on oxygen (O2) conditions, and variable concentrations of O2 can affect the stability of soil C (Li et al., 2021). Microbial organisms reduce Fe and Mn in low oxygen conditions through less-efficient anaerobic respiration and release C into porewaters of the soil. On the other side, oxidation of Fe and Mn creates reactive oxygen species that are electron seeking. These species interact with the soil and can produce significant amounts of CO2 (Liu et al., 2023). We hypothesized that the anthropogenically produced legacy sediment would act as a barrier for the diffusion of gases and nutrients and will decrease oxygen conditions at depth. These modified oxygen conditions will lower the redox potential of the buried A horizon and as a result, the iron redox cycle and the nutrients it cycles with, namely carbon, will be affected. To test our hypothesis, we performed large-scale field sampling and laboratory mesocosm experiments that were subjected to a variety of oxygen conditions and sediment thicknesses to attempt to simulate the conditions at our field site in a controlled environment.

Site Description

The Kessler Atmospheric and Ecological Field Station (KAEFS) is a 360 acre research site in the Permian Redbed region of Central Oklahoma (Figure 2). The

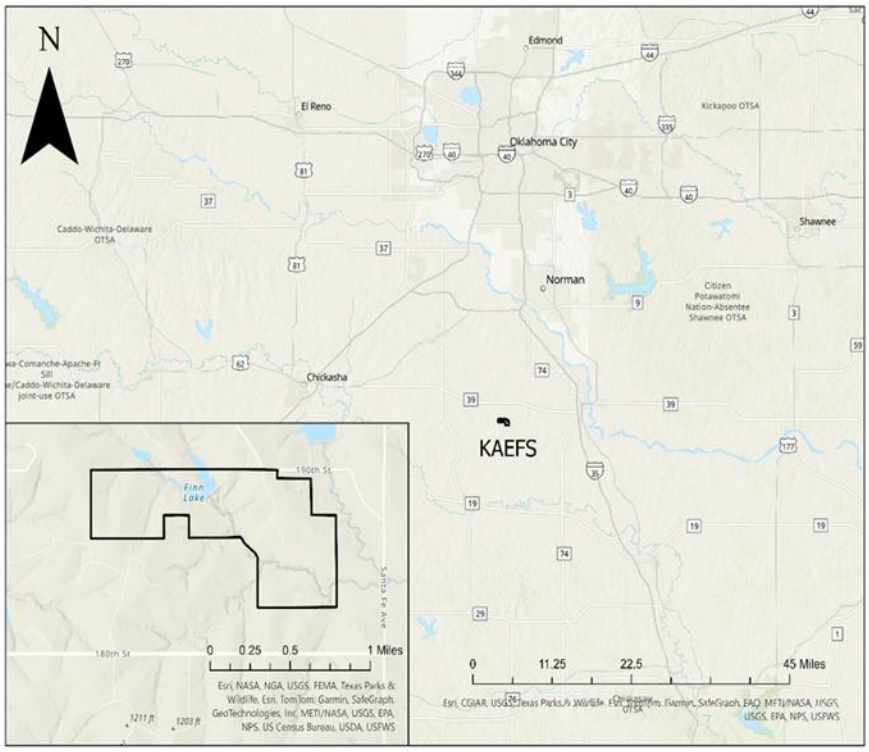

Figure 2: A map showing the location of the Kessler Atmospheric and Ecological Field Station (KAEFS) in Central Oklahoma as well as the modern day boundaries of the historic farm.

historic farm was originally allotted to a Choctaw family for homesteading in 1904. The farm has changed ownership several times before eventually being donated to the University of Oklahoma by its last owner, Dr. Edwin Kessler in 1988. Kessler performed many experiments at KAEFS focused on erosion and restoration of the prairie. Up until 1976, the land has been extensively grazed and cultivated, supporting cotton, corn, sorghum, peanuts, watermelons, and dairy cows. Land use at the site has eroded the hillslopes and incised the river bank nearly 2m. The historic floodplain at KAEFS is now hydrologically isolated from the historic stream bed and a layer of legacy sediment covers the A horizon of the floodplain soil.

The soils at KAEFS are mollisols, which are grassland soils that have surface A Horizon that is deep and nutrient-rich. The molliosols at the site are derived from Permian rocks that are nutrient-rich and their red color is from the iron oxides in the source rock. The texture of the soils at our sampling areas ranges from Loamy Sand to Clay Loam depending on depth and are part of the fertile Nash-Lucien series. The

loamy texture allows soils to retain moisture to be used by deep-rooting plants, but is able to quickly drain away to prevent waterlogging. Since the farm has only been cultivated and grazed in the last century, the native prairie tallgrasses stored considerable amounts of organic matter before anthropogenic activity began.

Methods

Initial Sampling of KAEFS

First, to determine whether the buried horizons are associated with evidence of Fe redox cycling, we sampled the soils in the historic floodplain at KAEFS. Soils were sampled directly north from the historic stream bank along a transect approximately 90 degrees from the streambed (Figure 3). Five profiles were taken altogether in 20 meter increments with names: “0m, 20m, 40m, 60m, and 80m”. Soils taken directly from the historic stream bank were labeled the 0m profile and the furthest soils away were the 80m. Within each profile, the samples were taken in 10cm increments of depth with a hand auger. After auguring down 10cm, the soil within the auger was removed and placed into a plastic bag that was properly labeled and sealed immediately upon extraction to preserve the in-situ conditions. In each profile, the soil was sampled up to a maximum depth of 100cm, resulting in 10 separate bags of soil per profile. The bags were named with respect to their depth: “0-10cm, 10-20cm, etc.”

Upon returning to the lab, a gravimetric water content measurement was taken from every bag of soil. The bags were shaken to homogenize them, and 10 grams of soil was removed and placed into an aluminum weighing pan. The samples were then placed into an oven at 40 degrees C for several days until no water remained in the

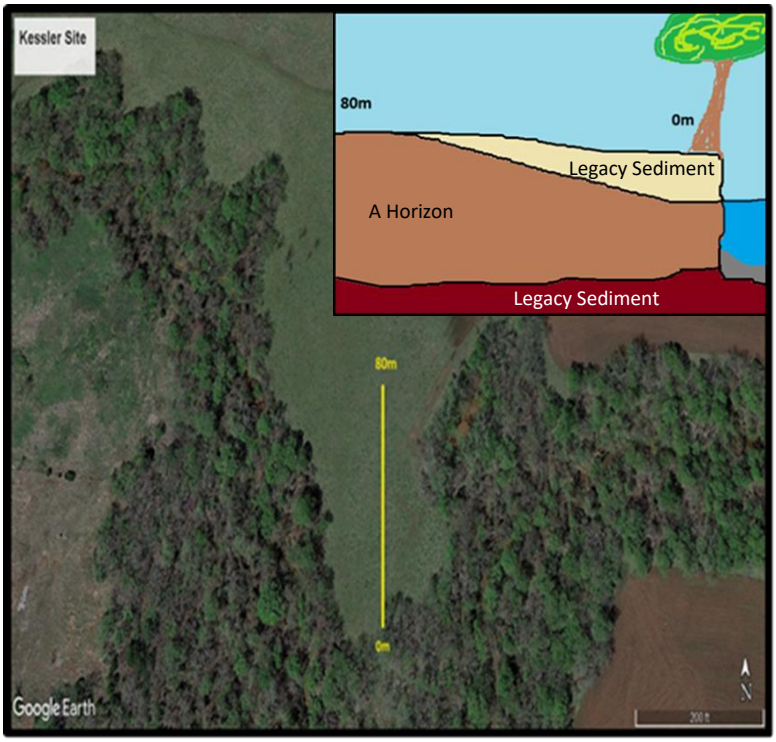

Figure 3: Transect at the historic floodplain of KAEFS. The tree line at 0 meters marks the incised channel that follows the floodplains shape. The conceptual model in the top right showcasing a cross-sectional view of the floodplain with the A horizon buried beneath a wedge of legacy sediment. The depth of burial increases as you approach the stream from the North.

samples. Another measurement was then taken and the total mass of the water was calculated and promptly converted into % mass water. These water content measurements are necessary to ensure that the water in pore space does not contribute to the mass of the soil when normalizing concentrations of analytes to the mass of the soil.

The next step in the process was performing HCl extractions on the soils that were collected. These extractions aimed to target soluble Fe (II) and Fe (III) found in poorly crystalline iron oxides. Two grams of soil were measured from each bag and placed into properly labeled 15mL polypropylene centrifuge tubes in triplicates, resulting in three tubes per one bag of soil. All of the resultant tubes were mixed with 14mL of 0.5M HCl and placed onto a shaking station for exactly 1.5 hours. After removal, the tubes were centrifuged for 10 minutes at 8000 rpm. The supernatant was then poured into fresh tubes for all samples, leaving the 2g soil pellets behind in the shaken tubes. The supernatant solutions were then used in the ferrozine method.

We determined the concentrations of both Fe (II) and total Fe in the HCl extractions using the ferrozine method. In the ferrozine method as adapted from (Huang

and Hall, 2017), the samples are prepared in a microplate to calculate the absorbance of each supernatant solution when reacted with the ferrozine reagent. Since the ferrozine reacts in the presence of soluble iron, the absorbance of the mixture directly corresponds to the iron concentration from the soils it was taken from. For each well in the microplate, the mixture was 40 microliters of supernatant, 40 microliters of either 10% hydroxylamine hydrochloride to determine the concentration of Fe (Total) or 1.8M HCl for measuring only Fe (II), and 200 microliters of ferrozine solution. The sample mixtures were run against known iron standards in the same 0.5M HCl matrix that were created beforehand. The plates were allowed to mix for 30 minutes in a dark container before they ran at 562nm and the absorbance values were obtained with a spectrophotometer. Then by combining concentration with known values of water content, soil mass, and volume of HCl, the concentration of mg Fe kg-1 soil was determined. By subtracting the values of Fe (II) from Fe (Total), we are able to additionally derive Fe (III).

Mesocosm Experiment

With the data obtained in the first step, we created a more controlled experiment to examine whether the depth of burial generated any detectable difference between different soil treatments. A series of mesocosms were constructed to house small representations of the soil found at the historic floodplain at KAEFS. Each mesocosm was constructed from a ¼ inch thick PVC pipe, was 4 inches in diameter, and 5 inches tall. A plumbing cap was placed on the bottom and carefully adhered using PVC cement so that the primer and glue would not interface with the experiment at all. All pieces used in constructing the mesocosm went through a strict acid wash cycle utilizing 0.5M

HCl and ultra-pure water. There were 18 mesocosms in total constructed for the lab experiment and they were divided into three equal groups based on oxygen conditions. The first 6 were labeled ‘anoxic’ the next 6 were labeled ‘fluctuating,’ and the last 6 were labeled ‘oxic.’ In each of the three groups, half of them were covered with 150g of sediment and the other half were covered with 300g of sediment. This meant that every combination of oxygen condition and sediment cover had 3 replicates. Anoxic mesocosms were placed in an anaerobic chamber with a composition of 5% hydrogen and 95% nitrogen and remained inside for the duration of the experiment. Fluctuating mesocosms were kept in the chamber for 4 days out of a week and allowed to reoxygenate under ambient laboratory conditions for 3 days before being sampled. The oxic mesocosms were kept uncovered in open air for the duration of the experiment. All containers were given water in an amount of ~75% water-filled pore space derived from the calculation in (Figure 4). Extractions were performed over the course of 13 weeks with sampling at regular intervals for consistency. Miniature soil cores were sampled from the mesocosms utilizing a syringe and the buried A horizon was separated to be used in HCl extractions.

$$WFPS = \frac{100 \times (\text{gravimetric water} \times \text{soil density})}{1 - (\text{soil density}/\text{soil particle density})}$$

Figure 4: The water-filled pore space calculation used to determine the amount of water the mesocosms were given. The soil particle density is assumed to be quartz as standard.

Soil Nitrate Extraction

To analyze the nitrate concentration of the soils, a new set of 2g soil cores were taken from the buried A horizon of the mesocosms using a syringe. The soil samples were immediately made into solutions so as to properly reflect the oxygen conditions of the containers they were taken from. The solutions were prepared utilizing the same extraction procedure as the ferrozine method detailed in the Iron vs Depth Experiment, but utilizing 2M KCl instead of 0.5M HCl. Upon successful creation of supernatant solutions, the nitrate concentrations were analyzed using the vanadium (III) method outlined in (Doane and and Horwáth, 2003). The nitrate concentrations were measured against standards created from a 70% nitric acid solution and 2M KCl.

Soil Elemental Combustion Analysis

Additional 1 gram samples were taken from each mesocosm, along with multiple 1 gram samples from an unaltered bag of soil that functions as an experimental control before any variability was added. These samples were placed into aluminum weight tins and placed into an oven at 40 degrees C for a week until they were completely dry and contained no water. These soils were then milled using steel balls into very fine particles over the course of several days. The milled soils were weighed on an analytical balance

into amounts of 40mg and carefully folded into small aluminum weighing tins. Utilizing a dry combustion method for total organic carbon, the samples were processed on a vario EL elementar carbon analyzer.

Mesocosm Cyclic Voltammetry

To further quantify the complex biogeochemistry created by different environments on the previously constructed mesocosms, an experiment was designed to measure redox potential under the simulated conditions. Using 2 thin graphite electrodes as the positive and negative electrodes and a silver electrode in a solution of silver-silver chloride, we performed 3 separate cyclic voltammetry experiments through a Wavenow potentiostat on mesocosms from each of the simulated environments, anoxic, fluctuating, and fully oxic. The potential was fixed with an upper bound of 800mV and a lower bound of -800mV and swept at a rate of 0.25mV/s over the course of 10 days. Each test was performed under the conditions that the mesocosm was exposed to over the course of the original experiment.

Manganese Analysis through ICP-OES

We filtered the supernatant solutions created in the mesocosm experiment, through no. 41 filter paper to remove any loose woody debris or roots that remained through the centrifuge process. Utilizing 15mL of each of the filtered solutions, we measured the concentration of extractable manganese through an ICP-OES. The samples were measured against Mn trace element standards using scandium. The calibration curve was calculated using standard procedure from the manufacturer.

Results

After sampling the cross section of the Kessler floodplain, the concentrations of Fe (II) were higher in profiles where the A horizon is buried, as opposed to profiles where it is at the surface (Figure 5). All values for this section are standardized and expressed as milligrams of iron per kilogram of soil. The Fe (II) values for buried profiles at Kessler ranged from 0.4 - 2.83 mg Fe kg^{-1} soil across the sampling days where the unburied profiles had a range of 0.21 – 2.03 mg Fe kg^{-1} soil. The buried profiles had increased concentrations at depth corresponding to the beginning of the buried A horizon (Figure 6). The depth profiles followed a similar trend in Fe (II) to each other across the floodplain with the unburied profiles having lower concentrations than the buried profiles at every point in the transect (Figure 6). The gravimetric water content for both the buried and unburied soils is within standard error of each other (Figure 7). At a depth of 20cm, the soil organic carbon (SOC) in the buried soil was 0.2% higher than in the unburied soil. This difference increased to

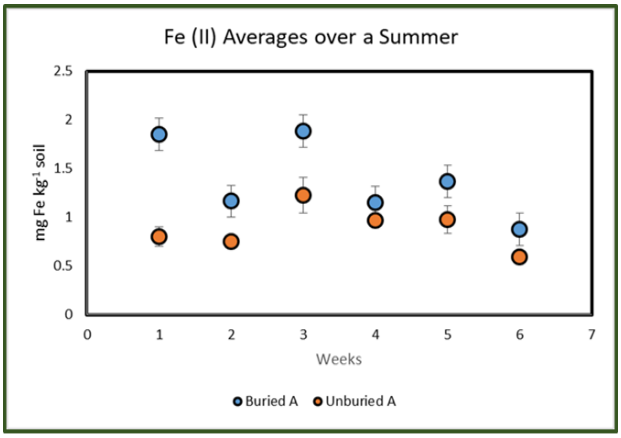

Figure 5: Averages of Fe (II) concentrations in the buried and unburied A Horizons from field sampling. Week 1 values were recorded immediately following a rainfall event.

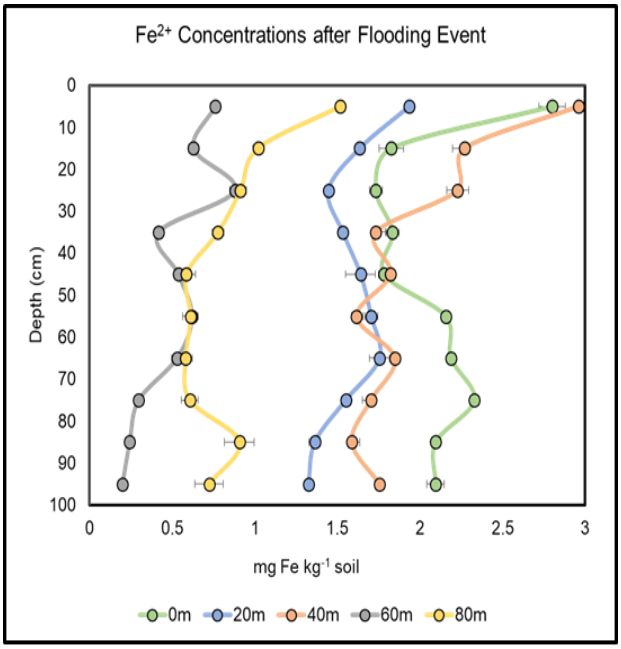

Figure 6: Data set used for the average values for the first week in Figure 5. 0m, 20m, and 40m buried soils show higher Fe 2+ concentrations than 60m and 80m unburied soils.

0.6% at a depth of 40cm. Finally the buried soil had 1% more SOC than the unburied at a depth of 60cm (Figure 8).

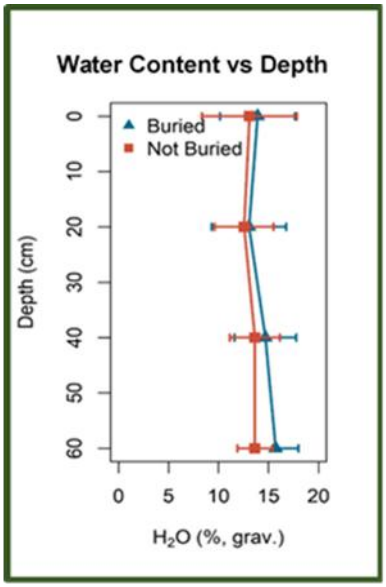

Figure 7: Average gravimetric water contents taken from buried and unburied profiles before drying for the ferrozine method. The water content is plotted with respect to depth.

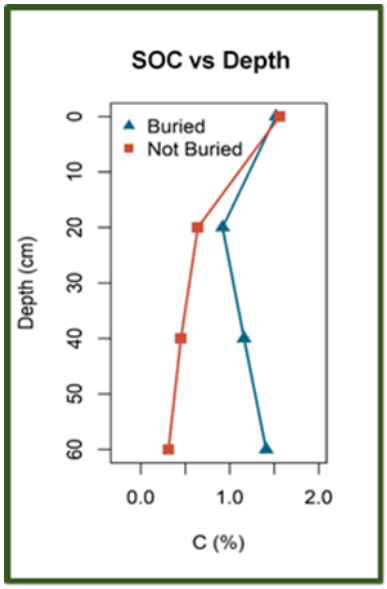

Figure 8: Average soil organic carbon taken from buried and unburied profiles utilizing the dry combustion method. The carbon is plotted with respect to depth.

In the mesocosm experiment, there was little to no variability in the Fe (II) concentrations in any of the buried A horizons in the mesocosms for the first five weeks, and the average stayed close to 2 mg Fe kg^{-1} soil (Figure 9). Fe (II) in the fluctuating and oxic mesocosms did not increase above 5 mg Fe kg^{-1} soil for the duration of the experiment. Fe (II) concentrations in the anoxic mesocosms rapidly increased over the next three weeks, reaching a peak 30 mg Fe kg^{-1} soil in week seven, roughly 15x greater than week five. The thicker sediment reached a slightly higher peak than the regular sediment at 32 mg Fe kg^{-1} soil but peaked a week later. The anoxic mesocosms dropped down to 6 mg Fe kg^{-1} soil in week nine. The regular sediment cover mesocosms climbed to two additional peaks at 8 mg Fe kg^{-1} soil in weeks ten and thirteen that were much smaller in magnitude than the initial peak seen at week seven. The mesocosms with thicker cover continued to

decrease to around 2 mg Fe kg^{-1} soil in week twelve, before climbing to its second and last peak at 12 mg Fe kg^{-1} soil in week thirteen.

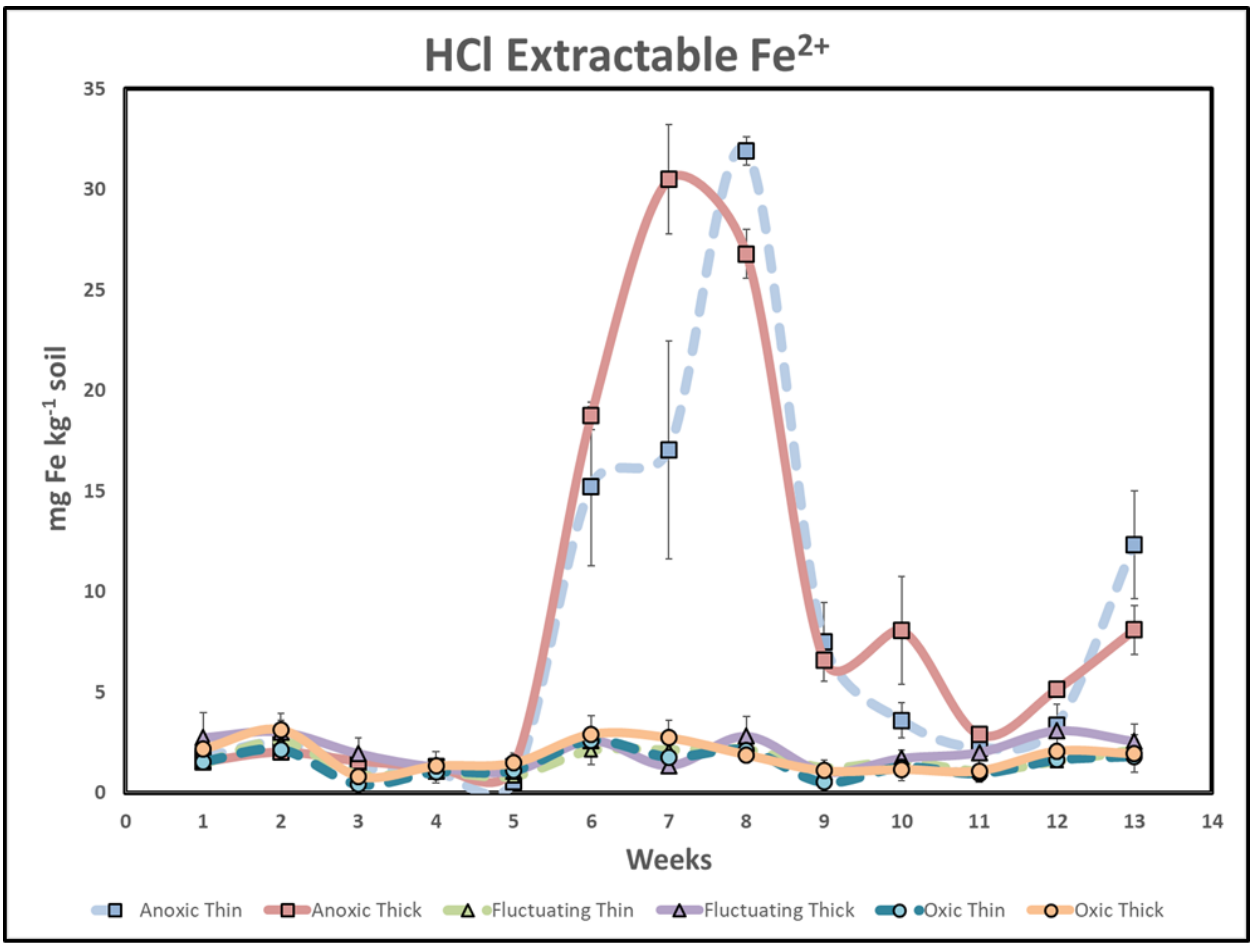

Figure 9: Average reduced iron concentrations extracted using the ferrozine method for each week of the mesocosm experiment plotted over the duration. Dashed lines indicate the thicker sediment cover and solid lines indicate the thinner sediment cover.

The Fe (III) concentrations began at 9 mg Fe kg^{-1} soil and decreased through the first four weeks to an average of 5 mg Fe kg^{-1} soil (Figure 10). All the mesocosms increased their Fe (III) concentrations slightly in week five to an average of 6 mg Fe kg^{-1} soil. All of the mesocosms then decreased in concentration with the anoxic mesocosms becoming completely depleted in Fe (III) for weeks six, seven, and eight. The fluctuating and oxic mesocosms increased in week eight to an average of 7 mg Fe kg^{-1} soil. The anoxic mesocosms increased in week

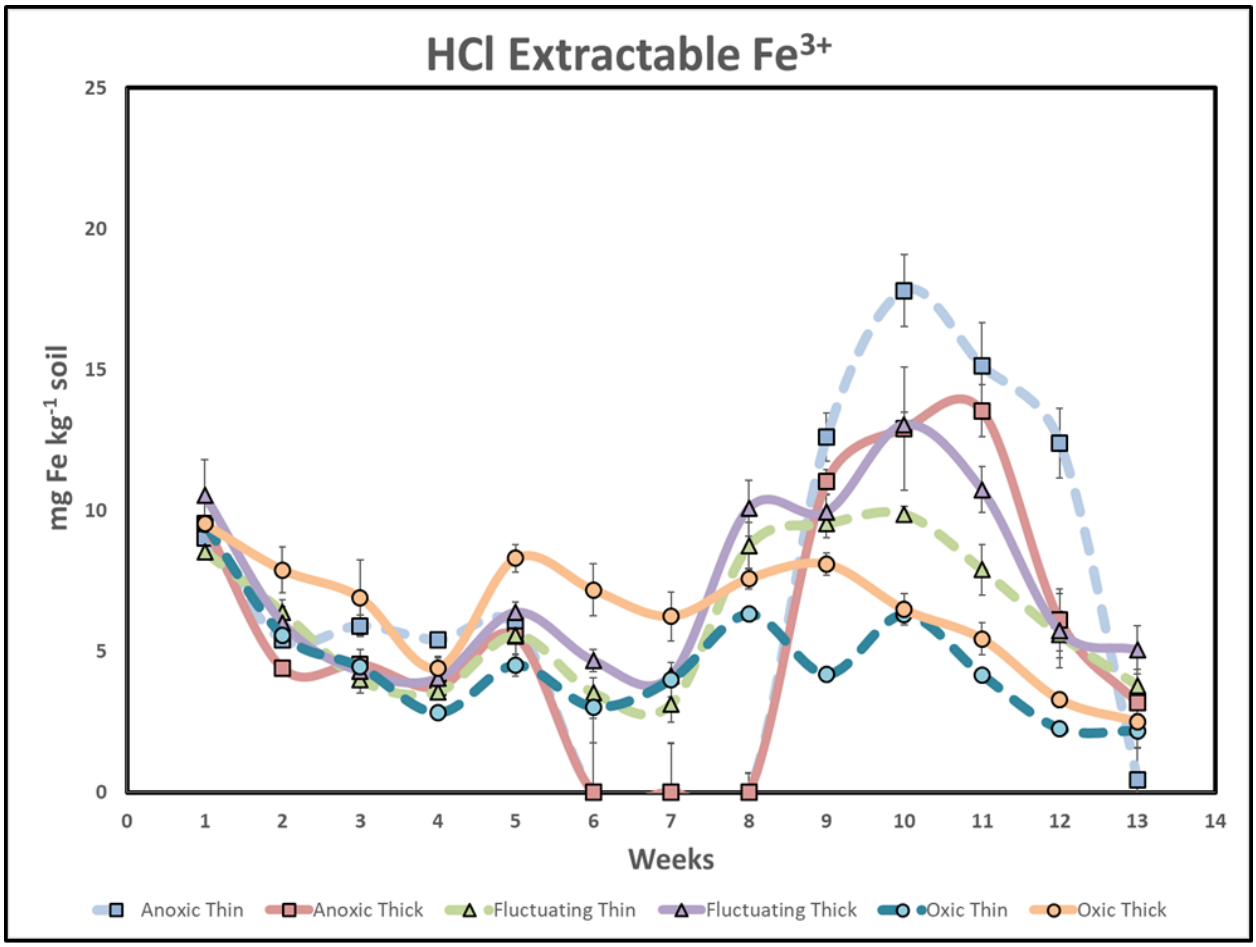

Figure 10: Average soluble oxidized iron concentrations extracted using the ferrozine method for each week of the mesocosm experiment plotted over the duration. Dashed lines indicate the thicker sediment cover and solid lines indicate the thinner sediment cover.

eight with an average value of around 14 mg Fe kg^{-1} soil and stayed higher than the fluctuating and oxic mesocosms. From week ten on, all mesocosms began to decrease in extractable Fe (III) significantly until the end of the experiment in week thirteen. All mesocosms ended at a lower concentration of Fe (III) than when the experiment began, and all but the anoxic mesocosms reached their lowest concentration across all weeks.

The total iron changed significantly across the duration of the mesocosm experiment (Figure 11). The total iron concentrations for all mesocosms decreased by 5 – 8mg over the course of the first four weeks. All mesocosms began to increase in

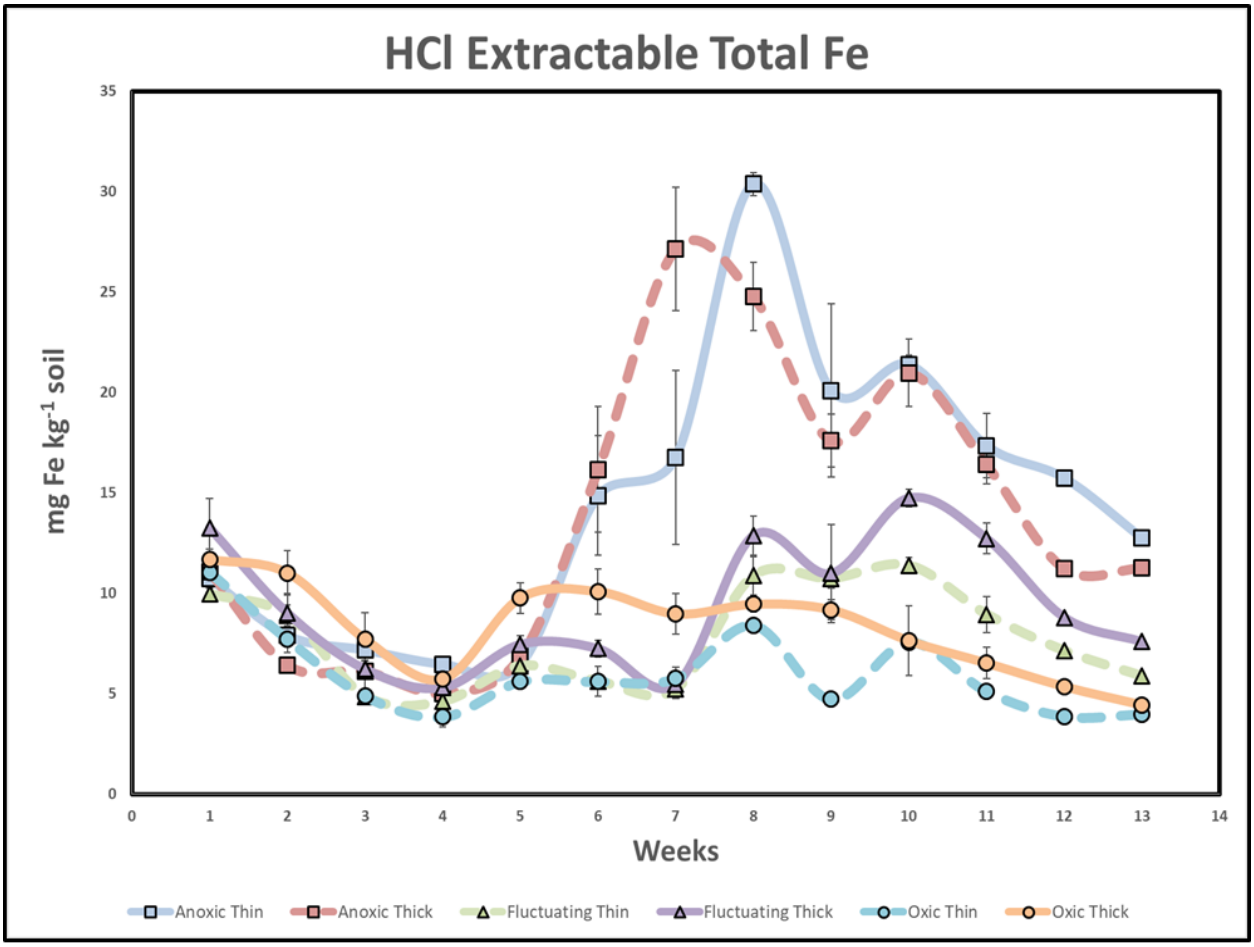

Figure 11: Average total iron [Fe (II) + Fe (III)] concentrations extracted using the ferrozine method for each week of the mesocosm experiment plotted over the duration. Dashed lines indicate the thicker sediment cover and solid lines indicate the thinner sediment cover.

concentration in week five to just below the initial before they began to differentiate based on oxygen state. The anoxic mesocosms increased in total iron dramatically in weeks six, seven, and eight, up to 3x higher than the initial iron. This corresponds with the significant iron reduction seen in (Figure 9) and the depletion of Fe (III) in (Figure 10). The total iron in the anoxic mesocosms dropped ~ 10 mg Fe kg^{-1} soil in week nine, before increasing again in week ten by ~ 5 mg Fe kg^{-1} soil. Over the final three weeks, the total iron in the anoxic mesocosms drops to a relative low of ~ 12 mg Fe kg^{-1} soil, finishing the experiment with barely more iron than it began. The thick fluctuating and the thin oxic mesocosms

followed a similar trend to the anoxic mesocosms, with much lower amplitudes. The thick fluctuating mesocosms reached a higher total iron concentration than the initial in week ten. The thin fluctuating mesocosms reached a higher total iron concentration than the initial in week eight. The fluctuating mesocosms climbed down to below the initial in week thirteen. The oxic mesocosms are the only samples to never return to the same iron concentration as the initial, cycling with lower amplitudes than any other mesocosm.

The percentage of nitrogen, carbon, and sulfur varied in accordance with the oxygen state of the mesocosm (Table 1). The nitrogen values for all mesocosms were higher than the beginning of the experiment with the anoxic mesocosms having ~ 0.5% more nitrogen. The same trend was observed for carbon with all mesocosms having

Table 1: percent element concentrations for nitrogen, carbon, and sulfur in the mesocosms. Replicates are averaged together for each subset. Data obtained utilizing a dry combustion method.

Sample	Whole Element Averages		
	% N	% C	% S
Anoxic Thin	**0.1233** ± 0.0033	**0.9933** ± 0.0348	**0.0890** ± 0.0053
Anoxic Thick	**0.1000** ± -	**0.9900** ± -	**0.0550** ± -
Fluctuating Thin	**0.1100** ± 0.0300	**1.2533** ± 0.3100	**0.0590** ± 0.0030
Fluctuating Thick	**0.0833** ± 0.0033	**0.9233** ± 0.0470	**0.0473** ± 0.0017
Oxic Thin	**0.0800** ± 0.0058	**0.9467** ± 0.0296	**0.0580** ± 0.0012
Oxic Thick	**0.0867** ± 0.0088	**1.0233** ± 0.0928	**0.0583** ± 0.0022
Control	**0.0720** ± 0.0066	**0.8820** ± 0.0663	**0.0542** ± 0.0023

increased carbon concentrations from the beginning. The minimum increase in carbon was ~0.04% in oxic mesocosms with thin sediment cover and the maximum increase

was ~0.4% in the fluctuating mesocosms with thin sediment cover. The fluctuating thin mesocosms did however have a significantly higher standard error of 0.3. There was not a noticeable change in elemental sulfur for any of the samples except the anoxic thin mesocosms which increased by nearly 60%. The concentrations of all three elements were higher in mesocosms with thin sediment cover for both the anoxic and fluctuating oxygen states. The difference in concentrations between the thin and thick sediment cover for the oxic mesocosms falls within standard error for all elements. Overall, all mesocosms were more concentrated in nitrogen than when the experiment began. Sulfur content had no noticeable change over the course of the experiment except in the Anoxic Thin mesocosms where it had a significant increase over all other treatments

Nitrate concentrations were diminished in the anoxic mesocosms with respect to both the fluctuating and the oxic mesocosms (Table 2). Nitrate was more than 20x greater in the fluctuating mesocosms than in the anoxic mesocosms. The concentrations of nitrate for the oxic mesocosms were significantly higher than the anoxic and the fluctuating, with the thicker sediment cover having nitrate concentrations that were over 200x greater than the anoxic mesocosms. While the nitrate in the regular sediment cover for the oxic mesocosm was 4x less than its thicker counterpart, the concentrations were still much larger than in other mesocosms. Manganese concentrations are considerably higher than the iron concentrations for all oxygen states in the mesocosm experiment (Figure 11). The anoxic mesocosms were on average 10x higher than the oxic samples, and 3x higher than the fluctuating samples. There is not much variability among each subset, and the values for each oxygen state are

consistent among the replicates. There is no significant difference in manganese concentrations between the thick sediment cover and the thin sediment cover mesocosms.

Table 2: Nitrate concentrations in the soil mesocosms expresses as mg NO3- per kg of dry soil. Concentrations were calculated from absorbance values obtained utilizing the Vanadium (IV) Chloride method from Doane and Horwath. Compared to the fluctuating and oxic values, the anoxic are nearly depleted in nitrate. Average manganese concentrations are from the end of the mesocosm experiment. The manganese concentrations correspond to the conditions in the mesocosms upon experiment completion. Concentrations are calculated from ICP-OES measurements and ran against manganese standards. Using the dry soil mass, the concentrations are then converted from ppm

Sample	Extractable Manganese and Nitrate (mg kg^{-1} soil)	
	Mn (Total)	NO_3^-
Anoxic Thin	**262.1052** ± 3.2089	**0.0182** ± 0.0029
Anoxic Thick	**286.3562** ± 3.6972	**0.0126** ± 0.0040
Fluctuating Thin	**92.5686** ± 1.0163	**0.4315** ± 0.0831
Fluctuating Thick	**98.7687** ± 1.1326	**0.4057** ± 0.0398
Oxic Thin	**29.0391** ± 0.2626	**3.1849** ± 0.0988
Oxic Thick	**45.3670** ± 0.4795	**0.7760** ± 0.0783

In the cyclic voltammetry experiment, the anoxic voltammogram had the most defined steady state, with little to no variance (Figure 12). The most pronounced activity is in the range of 100 – 400mV corresponding with the accepted redox potentials of both iron and manganese. Additionally, a small increase in activity is observable at -500mV.

The fluctuating voltammogram exhibits the same trend as the anoxic for the 100 – 500mV range but with a larger magnitude of current (Figure 12). The largest density of currents stops around -250mV with multiple strands going as far as -800mV. The

portion that goes past -250mV has much fewer overlapping points and does not follow the steady state pattern of the rest of the voltammagram. The oxic voltammagram has pronounced positive current in the 100 – 800mV range, with its highest currents being 400 – 800mV (Figure 12). The negative current is highest in the -500 – 0mV range, with the largest concentration of current being -500 to -200mV. Like the fluctuating data, the

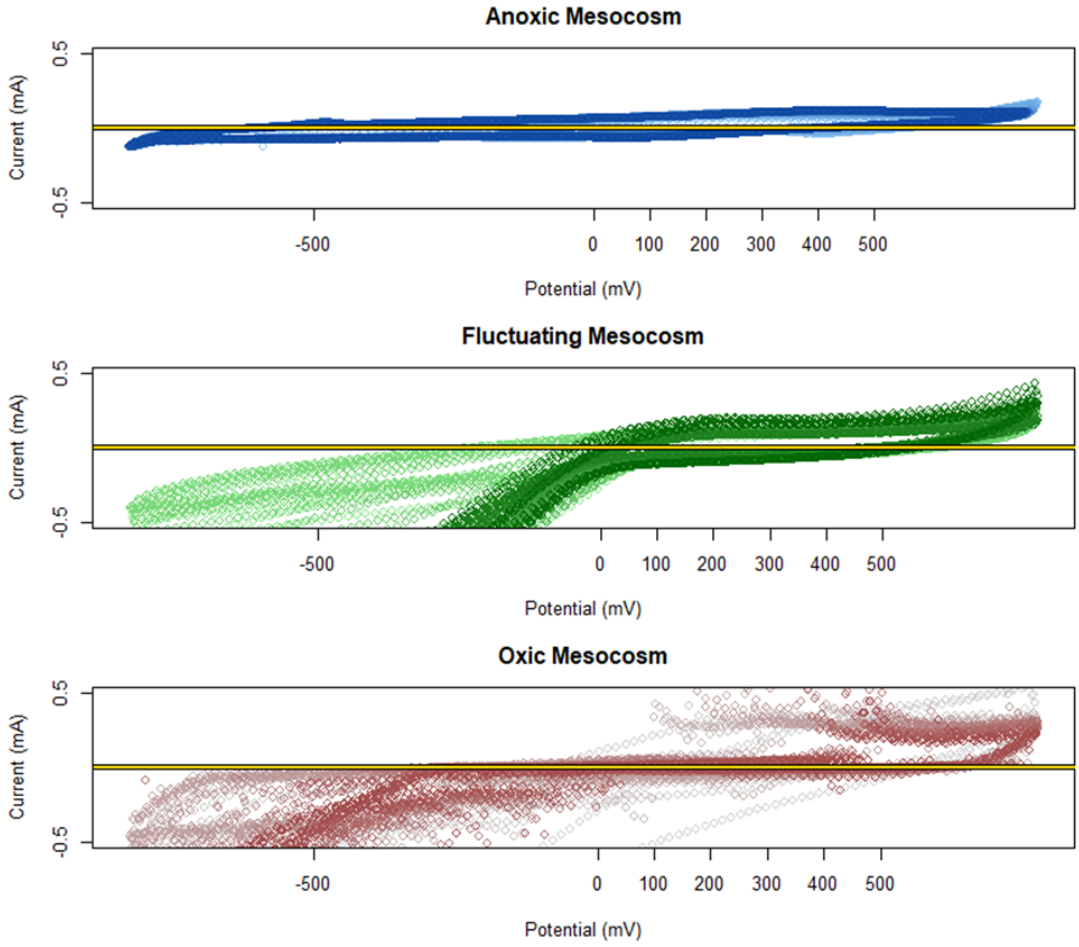

Figure 12: Cyclic Voltammetry Plots for one mesocosm from each oxygen treatment. The upper and lower bounds were 800mV and -800mV respectively. At a sweep rate of 0.25mV s-1, the experiment ran for 10 days. Positive current corresponds to oxidation and negative current corresponds to reduction.

oxic

voltammogram had lighter trends all over the graph and a large concentration of them around -800mV. The lighter colors at this range do not coincide with the darker shape formed from the other values.

For the initial cycles of voltammetry in the anoxic mesocosm, the current initially became positive at -500mV (Figure 13). The current increased in tandem with the redox potential and the current reached a peak of 0.15mA at a potential of 800mV. The current began to decrease and became negative at 550mV. The current briefly went

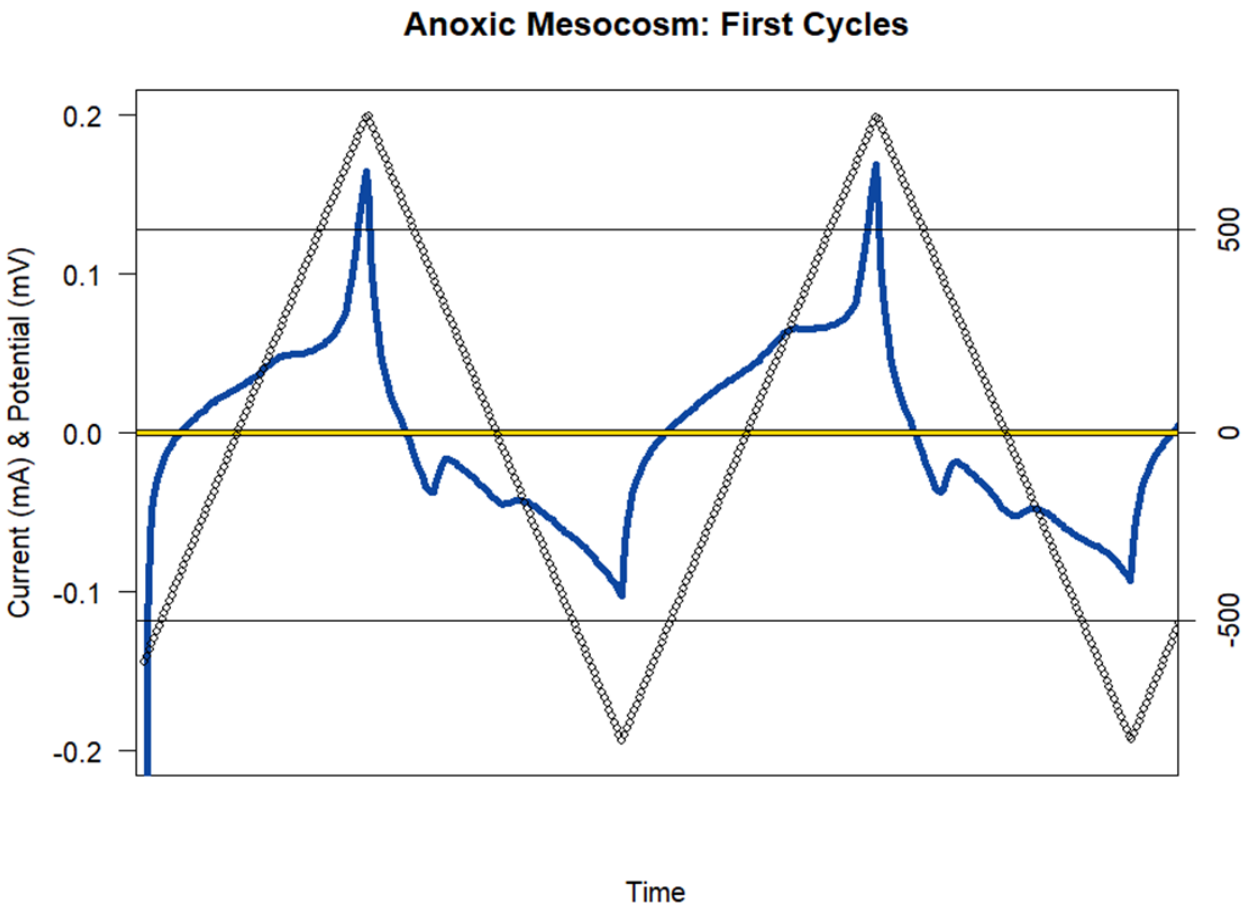

Figure 13: A voltammogram for the anoxic mesocosm that looks at the first few cycles of reduction/oxidation. The total time from left to right is ~3 hours. The dark blue is the measured current and the straight black lines are the redox potential. Values for current are on the left and values for redox potential are on the right.

upward at 500mV and began coming back down. From this small peak at 500mV, the redox potential rapidly dropped to 0mV before decreasing down to a low of -800mV along with current. This cycle repeated again with a nearly identical shape that followed the same trend as the current and potential for the first cycle.

In the fluctuating mesocosm, the current became positive at 100mV (Figure 14). The current and redox potential climbed together where they both reached a peak at 0.22mA and 800mV respectively. The current began to decrease and became negative at a redox potential of 550mV. Once the current reached -0.5mA at 500mV, it began to plateau as the redox potential dropped down to 100mV. The current then dropped straight down and became increasingly negative as the redox potential reached 0mV. The second cycle of the fluctuating mesocosm was similar to the first cycle except the

current became positive at a redox potential of 0mV and had a slightly higher magnitude as it reached the same peak.

In the oxic voltammagram, the current became positive at 200mV (Figure 15). The current followed a steep slope up as it reached its peak at 0.55mA at a redox

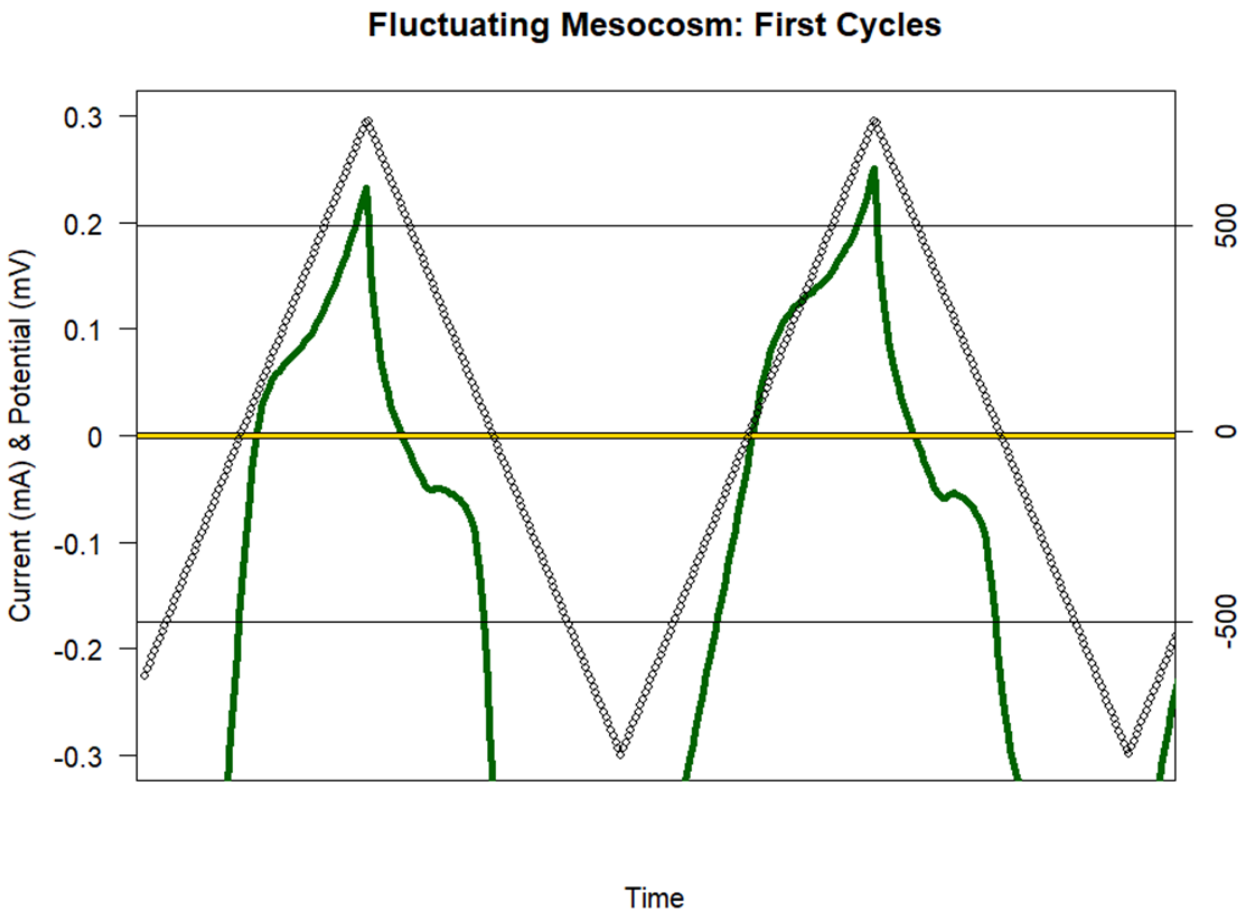

Figure 14: A voltammogram for the fluctuating mesocosm that looks at the first few cycles of reduction/oxidation. The total time from left to right is ~3 hours. The dark green is the measured current and the straight black lines are the redox potential. Values for current are on the left and values for redox potential are on the right.

potential of 800mV. The current steeply dropped after reaching the peak and became negative at 550mV. The current continued to drop, reaching 0.6mA at a redox potential of 150mV. The second cycle for the anoxic voltammogram is noticeably different from the first cycle. The current became positive again at a potential of -100mV. The current increased steeply then finally reached a peak of 0.58mA at 800mV. As the current

dropped from the peak, it abruptly changed directions back upwards before turning and continuing to decrease. The current became negative at 500mV and had a gentler slope than the first cycle. Current decreased slowly along with redox potential until the potential reached -400mV where the current plummeted further negative.

Discussion

The higher Fe (II) concentrations in the buried A horizon could correspond to limited oxygen diffusion through the legacy sediment, causing anoxia at different heights in the

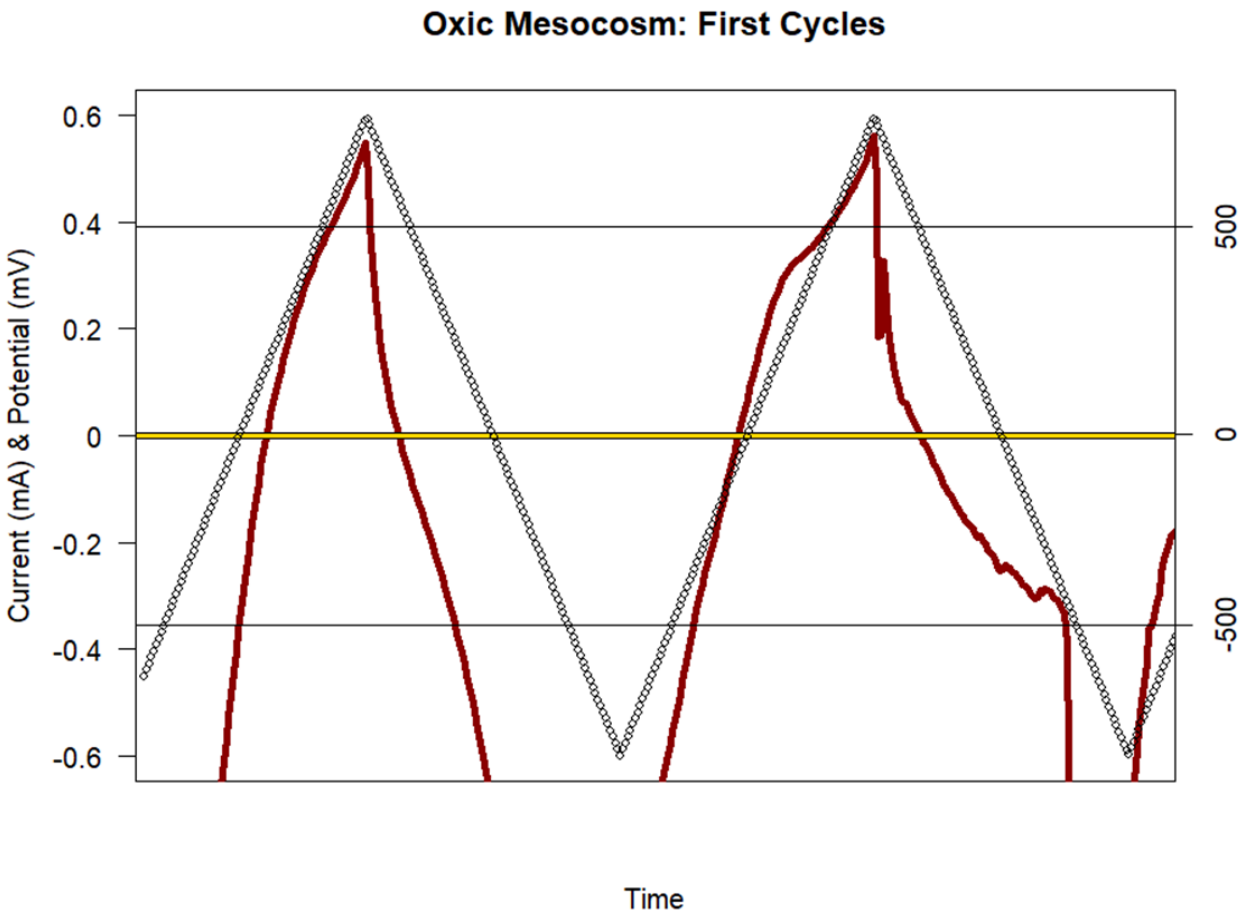

Figure 15: A voltammogram for the oxic mesocosm that looks at the first few cycles of reduction/oxidation. The total time from left to right is ~3 hours. The dark red is the measured current and the straight black lines are the redox potential. Values for current are on the left and values for redox potential are on the right.

A horizon (Figure 6). In unaltered mollisols, reducing conditions are created through high organic matter contents, limited oxygen diffusion, and brief flooding events (Scheffe et al., n.d.). Organic carbon is readily broken down in soils in accordance with the redox ladder. The more electropositive oxidants such as oxygen are utilized immediately in redox reactions near the surface where they are usually plentiful (Stumm, 1996). With increasing depth, less energy efficient oxidants are used with nitrate, manganese, iron, and sulfate being used respectively. When the buried soils at KAEFS receive rainfall, the conditions at depth become more reducing, resulting in a larger divide between the iron concentrations of the unburied and the buried soils in the first week (Stucki, 2011). Fe (III) oxides can be used by microorganisms as a terminal electron acceptor for anaerobic respiration. This process reduces Fe (III) into Fe (II) and mineralizes SOC into CO2. The dissolution of the solid iron releases nutrients that were sorbed, allowing them to be used by plants and soil microbes (Bonneville et al., 2004). The increased burial of the A horizon moves conditions towards more anoxia, allowing for increased carbon mineralization than in an unburied profile as there is more Fe (II) to facilitate the reaction.

Ginn et al. (2017) found that Fe (II) production was significantly increased in incubated soils that were subjected to fluctuating oxic conditions from 3 mmol – 45 mmol Fe (II) Kg-1 d-1. Their experiments record a cyclical nature of iron reduction that is re-oxidized with added oxygen and then reduced again with a higher amplitude than before. Their upland soils share similar characteristics of water saturation, organic matter, and oxygen inputs with the well-drained mollisols at KAEFS. They speculate that this trend can be attributed to the formation of easily reducible Fe (III) oxides that

appear as a consequence of continued dissolution and re-oxidation of autochthonous Fe (III) oxides.

Schulz et al. (2023) found that the amplitude of reductive dissolution of short range order iron oxides increased over time in an experiment with flooded paddy soil mesocosms. The Fe (II) associated with solid iron oxides was found in higher concentrations within the anoxic periods of the trial. Similarly to (Ginn et al., 2017), they attribute this to the formation of more easily reducible iron oxides with short range order as the oxygen is allowed to diffuse back into the soils. Additionally, they raised concerns over the potential consequences of these repeated redox cycles in regards to the increasing solubility of the newly formed iron oxides. As the frequency of reductive dissolution increases, trace elements found in minerals will be released at an increased rate.

Their research has implications for the soils found at KAEFS, since the soils are isolated from the nearby stream, and will receive drastically reduced nutrient recharge compared to naturally functioning floodplains. The deposition of fine, nutrient-rich sediments in a healthy and naturally functioning floodplain is the main way that the soil nutrients stay replenished (Gordon et al., 2020). Additionally, the inundation of a floodplain is a key component for regulating the concentrations of macronutrients such as phosphorous and nitrogen (Spink et al., 1998). In the absence of a functioning hydrologic regime, KAEFS is heavily reliant on microbial and plant activity to regulate and balance the nutrients in the soil. While the connectivity of a floodplain to a functioning fluvial regime does exert a significant control on floodplain ecology, KAEFS does still receive and drain rainfall quickly (Reckendorfer et al., 2013). The significant

sediment cover resulting in the burial of the A horizon is likely to prolong anoxia during flooding events. The increased interval of anoxia gives way to sustained Fe (II) reduction that is re-oxidized as it dries. If the processes at KAEFS are also creating increasing amounts of readily-reducible iron oxides, then the carbon stored in mineral associated organic matter may be being released in notably higher concentrations into the pore waters (Schulz et al., 2023).

In the mesocosms experiments, concentrations for both Fe (II) and Fe (III) show a steady decrease for the first several weeks of the experiment (Figures 8 & 9). The initial inactivity of iron cycling could be attributed to several factors. In accordance with the soil redox ladder, microbial organisms will utilize terminal electron acceptors in order of energy efficiency (Reddy and Patrick, 1978). Once oxygen is no longer available, microbial organisms will utilize nitrate, then Mn (IV), and then move on to Fe (III). The solid iron oxides are less energy efficient and as such, were not readily reduced until other more electropositive oxidants were consumed. This is supported by the nitrate extractions shown in (Table 2), where the mesocosms that were subjected to complete anoxia had nitrate concentrations near zero. Additionally, Mn (IV) is more readily reducible than Fe (III), and the large concentrations of HCl-extractable manganese in the anoxic and fluctuating mesocosms (Table 2) support the idea that manganese is influencing iron oxidation (Liu et al., 2022). Due its higher redox potential, Mn (IV) can undergo reductive dissolution by Fe (II). The coupled oxidation and dissolution through reduction has the ability to generate more intermediate reactive species that are able to break down and mineralize more carbon than through just manganese or carbon cycling alone (Liu et al., 2022).

In paddy soils, which share similar a redox potential and nutrient content as the soils at the KAEFS floodplain, iron and manganese have been observed to act as electron donors for the production of N_2 (Xu et al., 2021). The high nitrate contents of agriculturally productive paddy soils provide ample fuel for denitrification. In their study, they found that Fe (II), Mn (II), and NO3- decreased in concentration in anoxic soil treatments while the concentrations of Fe (III) and Mn (IV) increased. Additionally, they calculated that the total electron contribution to denitrification from manganese and iron was equal at 18% (Xu et al., 2021). Their data corresponds with the relative depletion of nitrate in the anoxic mesocosms, along with the delayed oxidation event for iron observed in week ten (Figure 10 & Table 2). The N_2 in the anaerobic chamber provides a pathway for N_2-fixation, which is able to resupply nitrate to the system as it is reduced in denitrification. Their observed values for electron contribution indicates that manganese and iron are operating equally in the environment, as opposed to iron redox cycling being dominant.

Another factor that can be taken into consideration is microbial lag time. Microbial populations are documented to have a delayed growth response when they undergo or experience an environmental change (Swinnen et al., 2004). The concept of microbial lag-time is well studied in the food industry, and is a trait that is shared amongst single-celled organisms. Studies involving iron-reducing bacteria in paddy soils has found that certain strains of microbial organisms require a build-up period of time following oxygen depletion before they not only become active, but become the dominant microorganism in their environment (Buchanan and Klawitter, 1992). The soils utilized for the mesocosms experiment were taken directly and placed into their containers almost

immediately after sampling. Although great care was taken to simulate the environment at KAEFS in a laboratory setting, the microorganisms would still most likely undergo a period of adjustment.

Another factor to consider is the types of iron minerals found in the soils at KAEFS and their origin. The parent material for the soils in the historic floodplain is Permian redbed sandstones. Iron oxides that are produced from these rocks are commonly unreactive and resist the formation of redoximorphic features. Early work presented aluminum substitution in the iron oxide crystal structure as a pathway for the minerals to resist reductive dissolution (Torrent et al., 1987). A recent study has provided strong evidence that the size of the hematite crystals, and their lower surface areas is the explanation for the poor reactivity of the iron oxides (Mack et al., 2019). The crystalline iron oxides such as hematite, goethite, and lepidocrocite require considerably more energy to dissolve or reduce than amorphous oxides like ferrihydrite, even for specialized microbes that can produce siderophores (Hori et al., 2015). Even as iron-reducing bacteria become prevalent in the soils, the initial reduction-dissolution of crystalline iron is not easily achievable in comparison to not only other more favorable oxidants, but to more accessible ferrihydrite.

Conclusion

The introduction of anthropogenically produced legacy sediment has had a significant impact on the soils at KAEFS. The burial of the A horizon has led to increased Fe (III) reduction and increased carbon mineralization at depth in the iron-manganese redox transition zone. Additionally, the Fe (III) reduction at KAEFS is not

necessarily tied to rainfall events that flood the porewater space of the soil, inducing anoxia but is shown to be amplified by them. The increased reduction of Fe (III) in buried soils is observable even in samples that were drained completely, supporting the idea that the legacy sediment at KAEFS is acting as a barrier for the diffusion of oxygen. The mesocosms recorded an anaerobic oxidation event midway through the experiment that corresponds with the relative depletion of the Fe (II). The high HCl-extractable manganese content supports the idea that manganese may be acting as an acceptor for direct electron transfer for iron oxidation. The higher redox potential manganese oxides underwent reductive dissolution early on in conjunction with the decomposition of organic matter. The depletion of nitrate with the surge in Fe (III) production suggests that iron may additionally be acting as an electron donor for denitrification. The same trend is observable in the fluctuating mesocosms with a lower magnitude. The increased concentrations of HCl-extractable manganese in the anoxic and fluctuating mesocosms supports the concept of increased reductive dissolution resulting from repeated reduction-oxidation events. The high concentrations of soluble manganese indicate that iron may not be the primary driver for anaerobic respiration and that manganese may be contributing equally or outpacing iron in terms of cycling key nutrients. The carbon concentrations for all buried soils were higher than when the experiment began, suggesting that the modified redox cycling stimulated by legacy sediment is also affecting the organic carbon.

Implications

While there was not a significant difference in terms of sediment cover for any of the oxygen treatments, the amplitude of redox and the trend for all of the mesocosms was

not uniform. The lab-controlled mesocosm experiment proved to be a cost-effective and scalable way to modify redox potential by utilizing an anaerobic chamber as a proxy for flooding events. Additionally, the treatments were able to be destructively sampled while still preserving the key feature at KAEFS which is the cover of legacy sediment. The cyclic voltammetry could be reasonably applied in-situ to observe real and dynamic redox potential over any kind of land cover.The methods provided for the experiment provide a framework to modify and test the effects of anthropogenic land use on soil ecosystems.Legacy sediment is widespread across the world with significant deposition in the agricultural zones of the United States and Europe. There has been considerable research on the physical properties of legacy sediment and how it already has and is continuing to change geomorphology, but there is a knowledge gap about how these geomorphologic changes are influencing the ecosystems around them. Legacy sediment has source to basin implications for sediment and nutrient transport, but it also has implications for localized systems like KAEFS. The effect that legacy sediment as on an environment is heavily dependent on the ecosystem it is affecting. Additional research is needed to assess the total range of geochemical changes that can occur due to legacy sediment.

Works Cited

Allan James, L., Beach, T.P., Richter, D.D., 2021. Floodplain and Terrace Legacy Sediment as a Widespread Record of Anthropogenic Geomorphic Change. Annals of the American Association of Geographers 111, 742–755. https://doi.org/10.1080/24694452.2020.1835460

Anderson, C.R., Davis, R.E., Bandolin, N.S., Baptista, A.M., Tebo, B.M., 2011. Analysis of in situ manganese(II) oxidation in the Columbia River and offshore plume: linking Aurantimonas and the associated microbial community to an active biogeochemical cycle. Environ Microbiol 13, 1561–1576. https://doi.org/10.1111/j.1462-2920.2011.02462.x

Bonneville, S., Van Cappellen, P., Behrends, T., 2004. Microbial reduction of iron(III) oxyhydroxides: effects of mineral solubility and availability. Chemical Geology 212, 255–268. https://doi.org/10.1016/j.chemgeo.2004.08.015

Buchanan, R.L., Klawitter, L.A., 1992. The effect of incubation temperature, initial pH, and sodium chloride on the growth kinetics of Escherichia coli O157:H7. Food Microbiology 9, 185–196. https://doi.org/10.1016/0740-0020(92)80046-7

Cotrufo, M.F., Lavallee, J.M., 2022. Soil organic matter formation, persistence, and functioning: A synthesis of current understanding to inform its conservation and regeneration, in: Advances in Agronomy. Elsevier, pp. 1–66. https://doi.org/10.1016/bs.agron.2021.11.002

Cotrufo, M.F., Ranalli, M.G., Haddix, M.L., Six, J., Lugato, E., 2019. Soil carbon storage informed by particulate and mineral-associated organic matter. Nat. Geosci. 12, 989–994. https://doi.org/10.1038/s41561-019-0484-6

Doane, T.A., and Horwáth, W.R., 2003. Spectrophotometric Determination of Nitrate with a Single Reagent. Analytical Letters 36, 2713–2722. https://doi.org/10.1081/AL-120024647

Dong, G., Han, R., Pan, Y., Zhang, C., Liu, Y., Wang, H., Ji, X., Dahlgren, R.A., Shang, X., Chen, Z., Zhang, M., 2021. Role of MnO2 in controlling iron and arsenic mobilization from illuminated flooded arsenic-enriched soils. Journal of Hazardous Materials 401, 123362. https://doi.org/10.1016/j.jhazmat.2020.123362

Ginn, B., Meile, C., Wilmoth, J., Tang, Y., Thompson, A., 2017. Rapid Iron Reduction Rates Are Stimulated by High-Amplitude Redox Fluctuations in a Tropical Forest Soil. Environ. Sci. Technol. 51, 3250–3259. https://doi.org/10.1021/acs.est.6b05709

Gordon, B.A., Dorothy, O., Lenhart, C.F., 2020. Nutrient Retention in Ecologically Functional Floodplains: A Review. Water 12, 2762. https://doi.org/10.3390/w12102762

Gougoulias, C., Clark, J.M., Shaw, L.J., 2014. The role of soil microbes in the global carbon cycle: tracking the below-ground microbial processing of plant-derived carbon for manipulating carbon dynamics in agricultural systems. Journal of the Science of Food and Agriculture 94, 2362–2371. https://doi.org/10.1002/jsfa.6577

Haque, K.M.S., Eberbach, P.L., Weston, L.A., Dyall-Smith, M., Howitt, J.A., 2015. Pore Mn2+ dynamics of the rhizosphere of flooded and non-flooded rice during a long wet and drying phase in two rice growing soils. Chemosphere 134, 16–24. https://doi.org/10.1016/j.chemosphere.2015.03.044

Hori, T., Aoyagi, T., Itoh, H., Narihiro, T., Oikawa, A., Suzuki, K., Ogata, A., Friedrich, M.W., Conrad, R., Kamagata, Y., 2015. Isolation of microorganisms involved in reduction of crystalline iron(III) oxides in natural environments. Front Microbiol 6, 386. https://doi.org/10.3389/fmicb.2015.00386

Huang, W., Hall, S.J., 2017. Optimized high-throughput methods for quantifying iron biogeochemical dynamics in soil. Geoderma 306, 67–72. https://doi.org/10.1016/j.geoderma.2017.07.013

James, L.A., 2018. Ten conceptual models of large-scale legacy sedimentation – A review. Geomorphology 317, 199–217. https://doi.org/10.1016/j.geomorph.2018.05.021

Janzen, H.H., 2004. Carbon cycling in earth systems—a soil science perspective. Agriculture, Ecosystems & Environment 104, 399–417. https://doi.org/10.1016/j.agee.2004.01.040

Johnston, C.A., Groffman, P., Breshears, D.D., Cardon, Z.G., Currie, W., Emanuel, W., Gaudinski, J., Jackson, R.B., Lajtha, K., Nadelhoffer, K., Nelson Jr, D., Post, W.M., Retallack, G., Wielopolski, L., 2004. Carbon cycling in soil. Frontiers in Ecology and the Environment 2, 522–528. https://doi.org/10.1890/1540-9295(2004)002[0522:CCIS]2.0.CO;2

Jones, M.E., Nico, P.S., Ying, S., Regier, T., Thieme, J., Keiluweit, M., 2018. Manganese-Driven Carbon Oxidation at Oxic–Anoxic Interfaces. Environ. Sci. Technol. 52, 12349–12357. https://doi.org/10.1021/acs.est.8b03791

Krauskopf, K.B., 1957. Separation of manganese from iron in sedimentary processes. Geochimica et Cosmochimica Acta 12, 61–84. https://doi.org/10.1016/0016-7037(57)90018-2

Lal, R., 2004. Soil Carbon Sequestration Impacts on Global Climate Change and Food Security. Science 304, 1623–1627. https://doi.org/10.1126/science.1097396

Li, H., Santos, F., Butler, K., Herndon, E., 2021. A Critical Review on the Multiple Roles of Manganese in Stabilizing and Destabilizing Soil Organic Matter. Environ. Sci. Technol. 55, 12136–12152. https://doi.org/10.1021/acs.est.1c00299

Li, Y., Yu, S., Strong, J., Wang, H., 2012a. Are the biogeochemical cycles of carbon, nitrogen, sulfur, and phosphorus driven by the “FeIII–FeII redox wheel” in dynamic redox environments? J Soils Sediments 12, 683–693. https://doi.org/10.1007/s11368-012-0507-z

Liu, J., Chen, Q., Yang, Y., Wei, H., Laipan, M., Zhu, R., He, H., Hochella, M.F., 2022. Coupled redox cycling of Fe and Mn in the environment: The complex interplay of solution species with Fe- and Mn-(oxyhydr)oxide crystallization and transformation. Earth-Science Reviews 232, 104105. https://doi.org/10.1016/j.earscirev.2022.104105

Liu, L., Ciais, P., Wu, M., Padrón, R.S., Friedlingstein, P., Schwaab, J., Gudmundsson, L., Seneviratne, S.I., 2023. Increasingly negative tropical water–interannual CO2 growth rate coupling. Nature 618, 755–760. https://doi.org/10.1038/s41586-023-06056-x

Mack, S.C., Rabenhorst, M.C., Berkowitz, J.F., 2019. Understanding the Inhibition of Color Change in Problematic Red Parent Material Hydric Soils. Soil Science Soc of Amer J 83, 838–847. https://doi.org/10.2136/sssaj2018.10.0390

Reckendorfer, W., Funk, A., Gschöpf, C., Hein, T., Schiemer, F., 2013. Aquatic ecosystem functions of an isolated floodplain and their implications for flood retention and management. Journal of Applied Ecology 50, 119–128. https://doi.org/10.1111/1365-2664.12029

Reddy, K.R., Patrick, W.H., 1978. Residual Fertilizer Nitrogen in a Flooded Rice Soil. Soil Science Soc of Amer J 42, 316–318. https://doi.org/10.2136/sssaj1978.03615995004200020023x

Rout, G.R., Sahoo, S., 2015. ROLE OF IRON IN PLANT GROWTH AND METABOLISM. RAS 3, 1–24. https://doi.org/10.7831/ras.3.1

Scheffe, K., Shaw, J., Stolt, M., Weindorf, D., n.d. Illustrated Guide to Soil Taxonomy.

Schulz, K., Notini, L., Grigg, A., Kubeneck, L., Wisawapipat, W., Thomasarrigo, L., Kretzschmar, R., 2023. Contact with soil impacts ferrihydrite and lepidocrocite transformations during redox cycling in a paddy soil. Environmental Science: Processes & Impacts 25. https://doi.org/10.1039/D3EM00314K

Spink, A., Sparks, R.E., Van Oorschot, M., Verhoeven, J.T.A., 1998. Nutrient dynamics of large river floodplains. Regulated Rivers: Research & Management 14, 203–216. https://doi.org/10.1002/(SICI)1099-1646(199803/04)14:2<203::AID-RRR498>3.0.CO;2-7

Stucki, J.W., 2011. A review of the effects of iron redox cycles on smectite properties. Comptes Rendus. Géoscience 343, 199–209. https://doi.org/10.1016/j.crte.2010.10.008

Stumm, W., 1996. Aquatic chemistry : chemical equilibria and rates in natural waters. New York : Wiley.

Swinnen, I.A.M., Bernaerts, K., Dens, E.J.J., Geeraerd, A.H., Van Impe, J.F., 2004. Predictive modelling of the microbial lag phase: a review. International Journal of Food Microbiology 94, 137–159. https://doi.org/10.1016/j.ijfoodmicro.2004.01.006

Swinnen, W., Broothaerts, N., Hoevers, R., Verstraeten, G., 2020. Anthropogenic legacy effects control sediment and organic carbon storage in temperate river floodplains. CATENA 195, 104897. https://doi.org/10.1016/j.catena.2020.104897

Torrent, J., Schwertmann, U., Barron, V., 1987. The reductive dissolution of synthetic goethite and hematite in dithionite. Clay Minerals 22, 329–337. https://doi.org/10.1180/claymin.1987.022.3.07

Wohl, E., Merritts, D.J., 2007. What Is a Natural River? Geography Compass 1, 871–900. https://doi.org/10.1111/j.1749-8198.2007.00049.x

Xu, B., Shi, L., Zhong, H., Wang, K., 2021. Investigation of Fe(II) and Mn(II) involved anoxic denitrification in agricultural soils with high manganese and iron contents. J Soils Sediments 21, 452–468. https://doi.org/10.1007/s11368-020-02776-z

Appendix

In-Situ Experiment

A significant portion of the original hypothesis involved in-situ sampling of the historic floodplain at KAEFS. To link the nutrient cycling with anthropogenically modified oxygen conditions, we devised an experiment to record these data without destructive sampling. The experimental design for this portion was to program and setup a CR1000x datalogger in the field to record gravimetric water content, soil conductivity, and O2 and CO2 concentrations in ppm. Due to differences in sensor instrumentation and the coding language of the datalogger, the CO2 sensors were ultimately abandoned. The O2 and water probes were installed in the field on a pole mount and were wired to a solar powered battery for continuous data sampling. Sensors were installed in doubles in the field with one of each going in the near surface of the soil, and the other going in depth in the buried A horizon. Along with machine calibrated sensors, physical soil gas sensors were installed alongside that could be sampled manually if there were any issues with the datalogger. Unfortunately, due to a communication failure between the site management team, and the site administration, the cables connected to the sensors were destroyed and the experiment was rendered non-operational. Data gathered from the datalogger before this incident is insignificant in sample size and in length of sampling and is not used in the thesis to draw any conclusions.